A Low-Cost Miniature Electrohydrostatic Actuator †

Travis Wiens * and Brendan Deibert

Department of Mechanical Engineering, University of Saskatchewan, Saskatoon, SK S7N 5A9, Canada;
bad176@mail.usask.ca

* Correspondence: t.wiens@usask.ca
† Presented at the First International Electronic Conference on Actuator Technology: Materials, Devices and
  Applications, 23–27 November 2020; Available online: https://iecat2020.sciforum.net/.

Abstract: This paper presents a low-cost, small-scale, electrohydrostatic actuator (EHA). This actuator leverages low-cost, mass-produced hydraulic components from the radio-controlled model industry, combined with a novel 3D printed valve. The system is capable of relatively high bandwidth operation, with much higher power- and force-density than comparable electrical actuators. This paper presents a dynamic system model, investigating the range of stability.

Keywords: hydraulics; fluid power; electrohydrostatic actuator; EHA

1. Introduction

There has been much recent research in the field of pump-controlled hydraulic actuators, also known as electrohydrostatic actuators (EHA) (see [1] for a recent review). These actuators promise higher efficiencies than valve-controlled actuators (with their associated losses across throttling valves). They can also offer advantages from a control point of view due to their linearity and load insensitivity. One configuration uses a variable-speed motor coupled to a fixed displacement pump (often a gear pump). If this is used to drive a single-rod cylinder, some facility for balancing the asymmetric flows must be included [2–8].

These actuators have commercial acceptance in the high power range, including current use for flight-control surfaces on Airbus A380 aircraft [9]. Commercial EHA units are available from a number of manufacturers [10].

In the small actuator range (i.e., displacements on the order of 50 mm and force capacity on the order of 50 N) electrical screw-driven actuators are common [11]. However, these actuators suffer from low force and power density, and high friction.

In recent years, small-scale hydraulic systems have become available, driven by radio-controlled model equipment (some would say "toys"). These systems feature small hydraulic cylinders driven by gear pumps driven by variable speed brushless DC or permanent magnet motors. The system is usually valve-controlled with the pump running at constant speed over a relief valve, resulting in an inefficient and load-sensitive circuit. This paper presents the application of these low-cost components in an EHA configuration. Previously, the lack of a suitable flow-balancing system made these systems economically impractical, so the major contribution of this project is a low-cost flow-balancing valve.

2. Materials and Methods

2.1. System Description

The prototype system is shown in Figure 1 and the schematic in Figure 2. The fixed displacement gear pump is driven by a variable-speed electric motor, in this case a permanent-magnet motor (commonly referred to as brushless DC, or BLDC). The pump and motor were purchased as a matched set, with a rated pressure of 4.5 MPa. For research purposes we drove the motor using an ODrive 24 V motor controller [12], but this could be easily replaced with a low-cost BLDC electronic speed-control (ESC) unit.
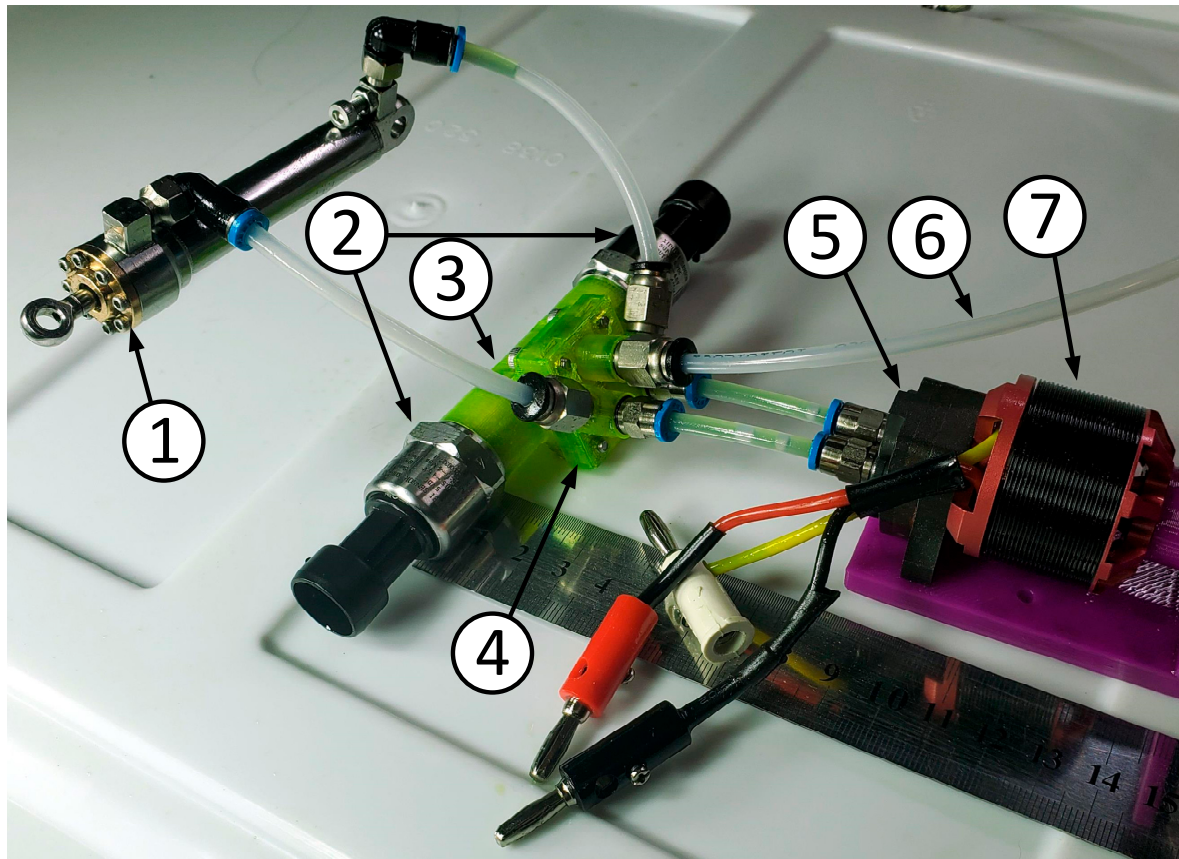

Figure 1. Photos of system, including (1) hydraulic cylinder, (2) pressure transducers, (3) 3D printed valve, (4) mounting plate, (5) pump, (6) charge pump line, and (7) motor. A cm ruler is included for scale. (Note that this photo was taken before bleeding air from the system.).
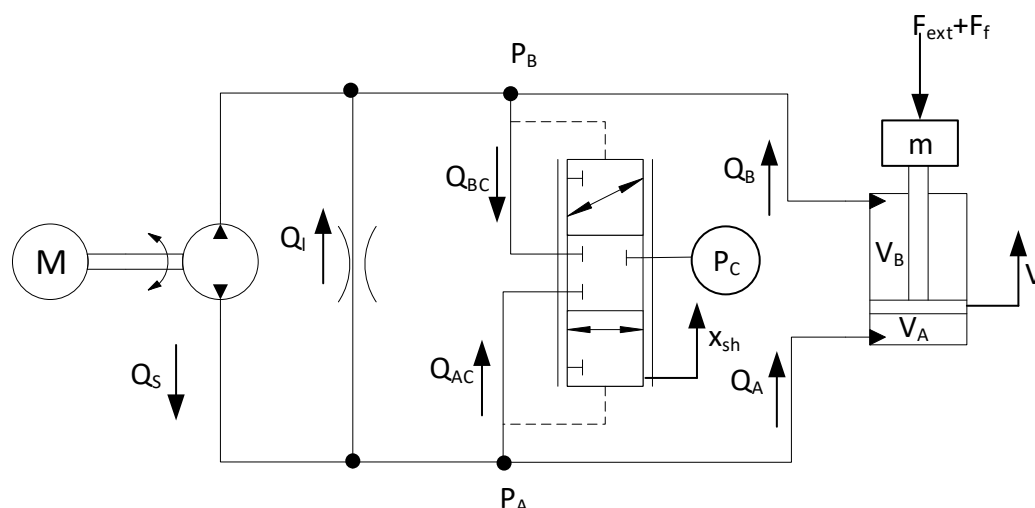
Figure 2. System schematic and nomenclature.

A commercially purchased hydraulic cylinder was used as the actuator, with 10 mm bore diameter, 4 mm rod diameter and 50 mm stroke. This cylinder was provided without a technical datasheet, but appears to have a hard, low-friction piston seal (perhaps polytetrafluoroethylene, PTFE) and has a soft elastomeric rod seal, likely nitrile rubber.

The single asymmetric hydraulic cylinder's unbalanced flow is handled by the inverse shuttle valve, shown in Figure 3. This valve connects the cylinder port with the lower pressure to the low-pressure supply. For testing purposes, this low pressure was supplied by an external pump, but it is believed that it would be possible for this to be replaced with a reservoir or accumulator [13]. The valve casing was 3D-printed from polyethylene terephthalate glycol-modified (PETG) using a Prusa i3 mk3 fused filament printer, at a layer height of 0.10 mm and 100% infill. The casing was produced with optional pressure transducers forming end caps, threaded into printed threads. The captured spool was printed in place, a layout that cannot be realized without using additive manufacturing. The authors believe this is the first hydraulic valve to require neither assembly nor finish machining. This design uses two connected hemispherical poppets that seat into conical seats. The hemispherical shape allows for good sealing even with angular misalignment of the unguided poppet. Once designed, the cost to produce this valve is nearly negligible, with a material cost of less than US$ 1 and requiring less than 4 hours of unattended printing time. For those without access to a 3D printer, numerous commercial enterprises can produce this part at minimal cost. We received commercial quotes for single quantities as low as US$ 13 plus shipping and less than US$ 2 in bulk quantities.
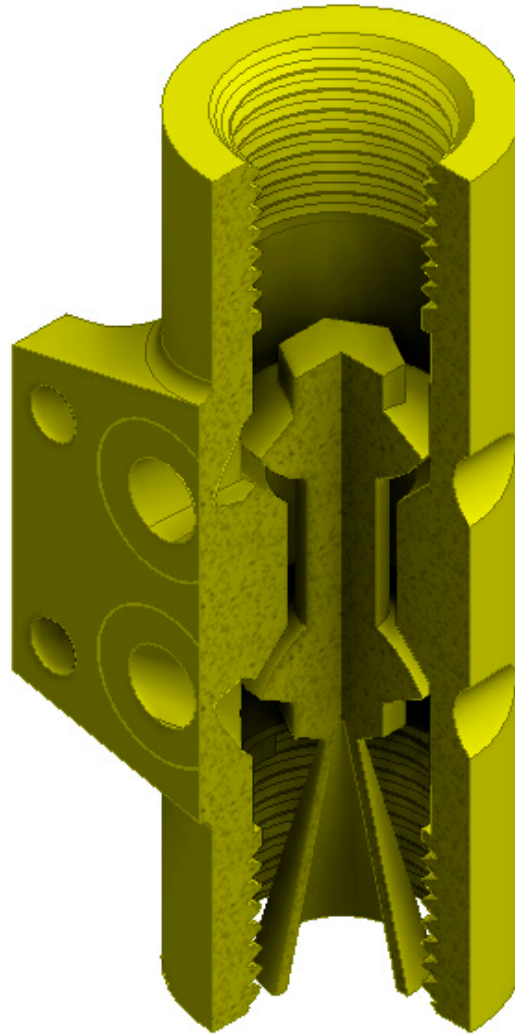
Figure 3. Cutaway view of the 3D-printed PETG valve. The conical structure at the bottom is a support required during printing and is removed by gripping the hexagonal shape on the top of the spool and twisting. For both valves, pressures P_A and P_B are connected via passageways through the casing (not clearly visible here) to the top and bottom chambers, and the charge pressure P_C is connected to the center of the casing between the two hemispherical sealing surfaces. 3D-printed threads at the top and bottom accommodate pressure transducers for the prototype valve, which may be eliminated if not required.

All connecting lines are nylon tubing, rated for 4 MPa, which sets the safe working pressure of the system. Rather than physical relief valves to enforce this pressure limit, we used the measured pressure to limit the pump velocity for this prototype. This system is not entirely reliable, so rupture discs or other weak points could be included in a production version to ensure safety. Alternatively, the motor current could be limited in order to limit pressure if pressure measurement was not required.

A previous paper [13] evaluated the steady state performance of the system and found it to have a very high specific force and power when compared to electrical actuators.

2.2. Dynamic Model

This section presents a dynamic model for the system, using nomenclature shown in Figure 2. Starting at the load, a force balance on the piston and attached mass gives

$$m\frac{dV}{dt} = P_A A_A - P_B A_B - F_{ext} - F_f \tag{1}$$

where A_A and A_B are the piston areas on the head and rod end, F_{ext} is the externally applied force, V is the actuator velocity and, following an equation modified from [14], the effective friction force is given by

$$F_f = (F_c + K_{PB}\mu P_B)tanh\left(\frac{V}{V_f}\right) + K_B \mu V \tag{2}$$

where F_c is the Coulomb Friction, μ is the dynamic viscosity, K_{PB} is a pressure-dependent friction term, K_B is a viscous damping term and V_f is a scale for "small" velocities (this tanh term is used to avoid numerical instability around zero velocity). Fluid friction in lines and fittings is also lumped into K_B (which should have a small effect). We investigated including a turbulent friction term (proportional to V^2) but found its value to be statistically indistinguishable from zero in experimental tests. Likewise, a P_A friction term was considered but was also indistinguishable from zero, likely due to the hard piston seal, as compared to the deformable elastomeric rod gland seal.

Assuming constant effective bulk modulus, β, in the fluid and containing passageways, continuity requires

$$\frac{V_A}{\beta}\frac{dP_A}{dt} = Q_s - Q_l - Q_{AC} - VA_A \tag{3}$$

$$\frac{V_B}{\beta}\frac{dP_B}{dt} = -Q_s + Q_l - Q_{BC} + VA_B \tag{4}$$

where V_A and V_B are the effective compliant volumes (including valve bodies, lines, and piston chambers).

The shuttle valve spool is assumed to have laminar friction and flow forces are neglected, giving a force balance of

$$m_{sh}\frac{d^2x_{sh}}{dt^2} = (P_A - P_B)A_{sh} - B_{sh}\frac{dx_{sh}}{dt} \tag{5}$$

where m_{sh} is the spool's mass, A_{sh} is the symmetrical piston area, and B_{sh} is the damping coefficient. The minimum and maximum displacement are limited by x_{shmin} and x_{shmax}.

This model lumps all internal leakage (i.e., pump, valve, and cylinder) into Q_l and all external leakage and valve flow into Q_{AC} and Q_{BC}. Laminar internal leakage is given by

$$Q_l = \frac{P_A - P_B}{R_l} \tag{6}$$

where R_l is the leakage resistance. The external leakage and valve flows are given by

$$Q_{AC} = \frac{P_A - P_C}{R_{AC}} \tag{7}$$

$$Q_{BC} = \frac{P_B - P_C}{R_{BC}} \tag{8}$$

where R_{AC} and R_{BC} are the resistances, with conductances linearly varying with spool position

$$R_{AC}^{-1} = R_{ACl}^{-1} + R_{ACv}^{-1}\frac{x_{shmax} - x}{x_{shmax} - x_{shmin}} \tag{9}$$

$$R_{BC}^{-1} = R_{BCl}^{-1} + R_{BCv}^{-1}\frac{x - x_{shmin}}{x_{shmax} - x_{shmin}} \tag{10}$$

where R_{ACl} and R_{BCl} are the leakage resistances with the valve closed, and R_{ACv} and R_{BCv} are the resistances when fully open (including both valve orifices and passageway resistances). While the orifices are likely turbulent at partial opening, the fast-responding valve spends the vast majority of its time at either extreme where the resistance is either dominated by laminar leakage flow or laminar

pipe flow. The intermediate resistances are largely included as a convenience for the numerical solver and have little effect on the system dynamics.

Table 1 shows parameters used for the simulation study, some of which were experimentally estimated in a previous work [13].

Table 1. Model Parameters.

Parameter	Value
Head End Piston area A_A	78.5 mm²
Rod End Piston Area, A_B	66.0 mm²
Fluid Viscosity, μ	28.3 cP
Fluid Bulk Modulus, β	1.0 GPa
Load Friction Viscous Coefficient K_B	2.50×10^4 N/(m/s)/(Pa s)
Load Coulomb Friction, F_c	3.41 N
Load Pressure Friction Coefficient, K_{PB}	5.27×10^{-6} N/(m/s)/Pa
Friction reference velocity, V_f	0.01 mm/s
Load mass, m	1.25 kg
Internal Leakage Resistance R_l	1.23×10^{12} Pa/(m³/s)
External Leakage Resistance R_{ACl}	6.83×10^{14} Pa/(m³/s)
External Leakage Resistance R_{BCl}	2.41×10^{12} Pa/(m³/s)
Open Valve Resistance R_{AC}	1.11×10^{11} Pa/(m³/s)
Open Valve Resistance R_{BC}	5.29×10^9 Pa/(m³/s)
Shuttle Spool Piston Area, A_{sh}	50.3 mm²
Shuttle Spool Damping, D_{sh}	12.2 N/(m/s)
Shuttle Spool mass, m_{sh}	1.2 g
Maximum spool displacement, x_{shmax}	2 mm
Minimum spool displacement, x_{shmin}	−2 mm
P_A compressible volume, V_A	2.55 mL
P_B compressible volume, V_B	2.24 mL
Charge Pump Pressure, P_C	250 kPa
Main pump maximum flow, Q_{smax}	0.7 L/min

2.3. Controller

This section presents an open-loop velocity controller for the system. This is intended to be a minimum viable controller, intended to provide an indication of the stability and controllability of the system, rather than an optimized controller that would actually be used in practice.

First, the controller estimates the valve spool state, either in mode 1 ($P_A > P_B$) or mode 2 ($P_B > P_A$). In the ideal case this is simply

$$mode = \begin{cases} 1 & if\ P_A > P_B \\ 2 & otherwise \end{cases} \tag{8}$$

More complex realistic controllers would apply filters and/or hysteresis to prevent spurious mode switching due to measurement noise.

Based on the mode, the flow required to achieve the desired velocity, V_{ref}, is calculated, assuming no leakage:

$$Q_s = \begin{cases} V_{ref}A_A & if\ mode = 1 \\ V_{ref}A_B & otherwise \end{cases} \tag{8}$$

As the leakage is dependent on the measured pressures P_A and P_B, a practical controller could improve steady state accuracy by compensating for this leakage.

2.4. Simulation Studies

The above system of equations was implemented in Matlab Simulink. A input of $V_{ref} = 0$ was applied and the system was allowed to reach steady state. A step in reference velocity was then applied and the actuator velocity and pressures were recorded for a constant load force F_{ext}.

3. Results

Figure 4 shows representative step response results for a range of load forces and commanded velocities. Figure 5 shows an example of a limit cycle that can be excited under certain conditions, and Figure 6 shows a map of which operating points excite this limit cycle.

(**a**)

(**b**)

(**c**)

(**d**)

(**e**)   (**f**)
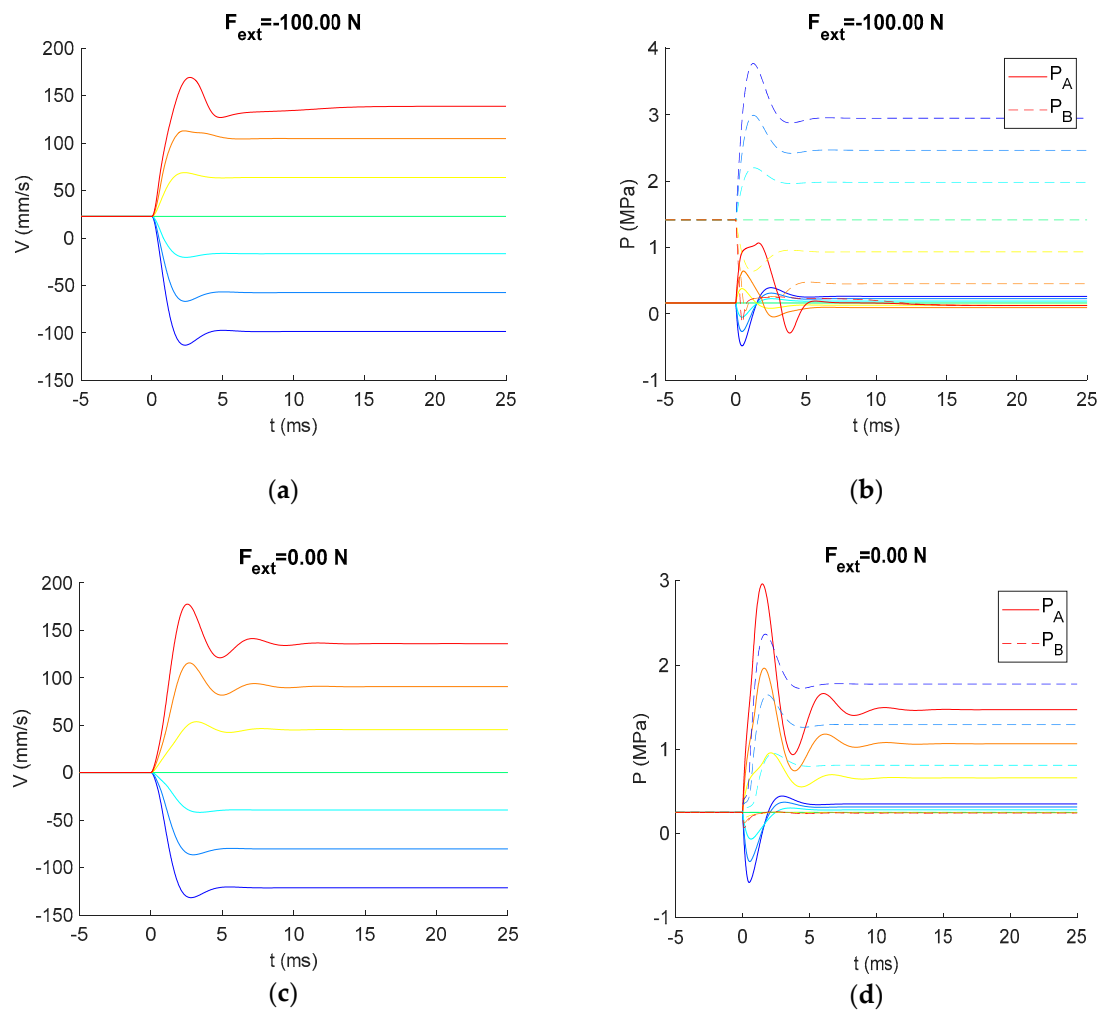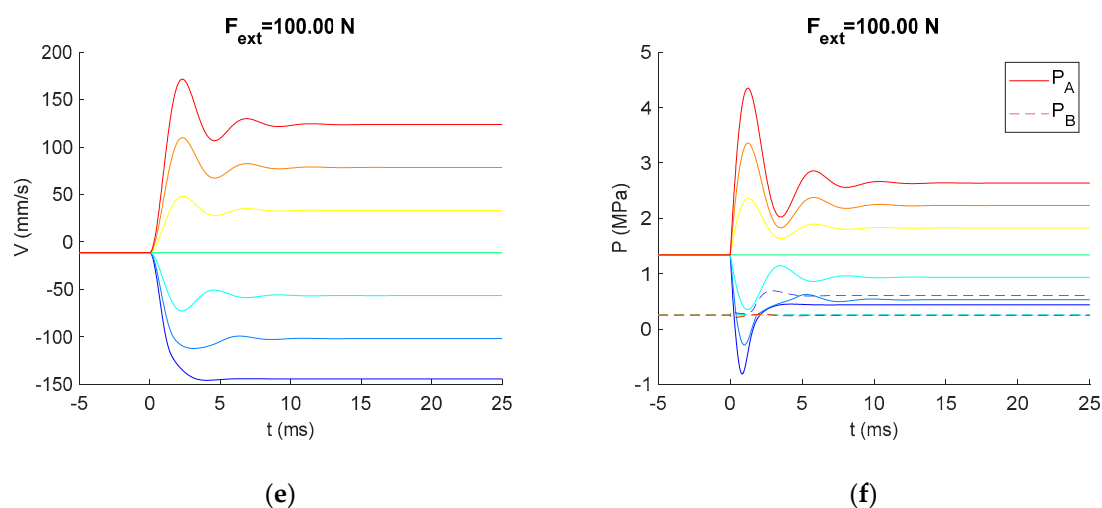
Figure 4. Example step responses, for a range of external load forces (different rows) and commanded velocities (different colors). Colors represent the same command velocity in each plot. Velocities are shown in (**a**), (**c**), (**e**) and pressures in (**b**), (**d**), (**f**).
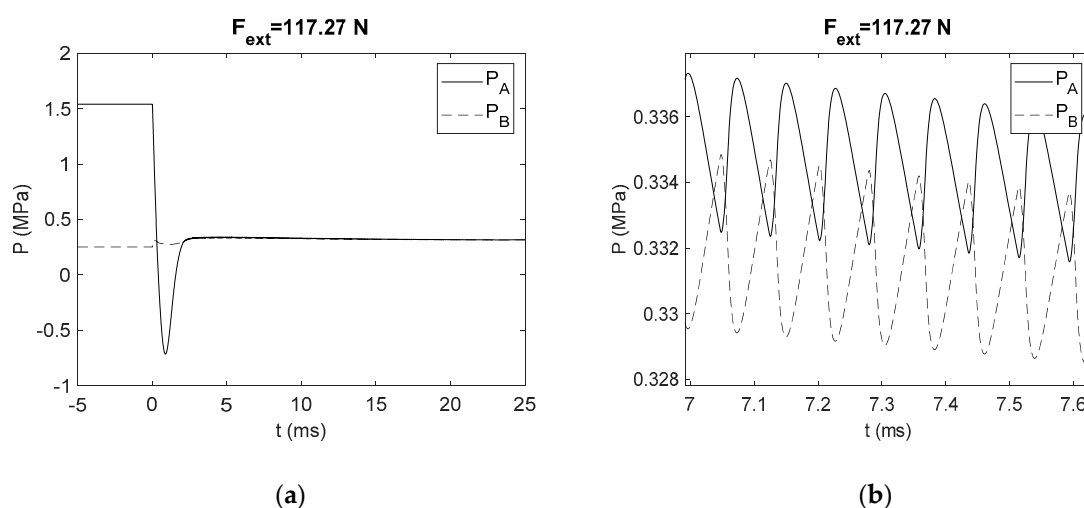

(**a**)   (**b**)

Figure 5. An example of a pressure limit cycle for $V_{ref} = -148.5$ mm/s and $F_{ext} = 117.3\ N$ (**a**), enlarged in Frame (**b**).
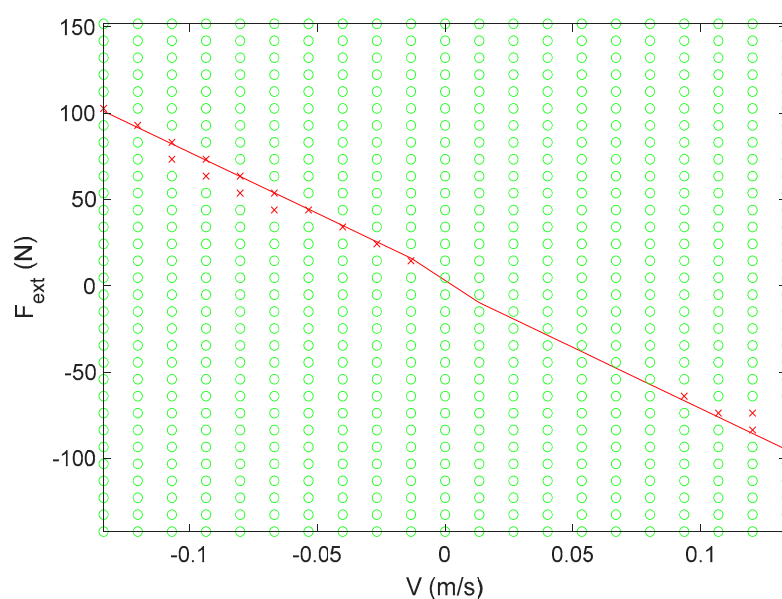
Figure 6. An oscillating pressure-limit cycle exists for the points denoted by a red x, while no oscillations exist for green circles. The red line denotes the critical load force where $P_A = P_B$ at equilibrium.

4. Discussion

As seen in Figure 4, the dynamic response is generally fast, and oscillations settle quickly. The nonlinear nature of the system can be observed as the velocity response's shape changes with operating point, with some responses overdamped and others showing some overshoot.

However, as shown in Figure 5, it is possible to excite a limit cycle, with the pressure continually oscillating. This instability has been identified in the literature [15–17] as being related to mode-switching of the shuttle valve spool around a critical external force when $P_A = P_B$. In [15], it is stated that the size of the unstable region around the critical force is related to the shuttle spool centering spring and orifice geometry. Following this theory, eliminating the spring (as in this paper) would represent an infinitesimal unstable zone. However, we still observe a small unstable zone, as shown in Figure 6. Luckily, this zone is very small, and it may be possible to mitigate the effects by adding leakage or pressure feedback [17].

5. Conclusions

This paper presents a dynamic model of a single-rod electrohydrostatic actuator with a novel 3D-printed shuttle valve. These dynamic results indicate that a known issue with stability is small with this valve, but is not entirely eliminated. Future work will further develop our understanding of the causes of this limit cycle with the aim of eliminated it. The dynamic model will also be used to optimize system parameters.

Abbreviations

The following abbreviations are used in this manuscript:

EHA   Electrohydrostatic Actuator

References

1. Ketelsen, S.; Padovani, D.; Andersen, T.O.; Ebbesen, M.K.; Schmidt, L. Classification and Review of Pump-Controlled Differential Cylinder Drives. *Energies* **2019**, *12*, 1293, doi:10.3390/en12071293.
2. Merritt, H.E. Hydraulic control systems. *J. Wiley* **1967**.
3. Ketelsen, S.; Kolks, G.; Andersen, T.O.; Schmidt, L.; Weber, J. Bootstrap Reservoir Concepts for Electro-Hydraulic Compact Cylinder Drives; 12th International Fluid Power Conference (12. IFK), Dresden, 12–14 October 2020.
4. Zhang, S.; A Minav, T.; Pietola, M. Decentralized Hydraulics for Micro Excavator. In Proceedings of the 13th International Modelica Conference, Regensburg, Germany, 4–6 March 2019, doi:10.3384/ecp17144187.
5. Wiens, T.; Bitner, D. An Efficient, High Performance and Low-Cost Energy Recovering Hydrostatic Linear Actuator Concept. In *BATH/ASME 2016 Symposium on Fluid Power and Motion Control*; Univeristy of Bath: Bath, UK, 2016.
6. Wiens, T. An efficient, compact and low-cost Dual Cylinder Hydrostatic Actuator (DCHA). *Int. J. Fluid Power* **2018**, *19*, 80–90, doi:10.1080/14399776.2018.1437321.
7. Achten, P.J.; Palmberg, J.O. What a difference a hole makes: The commercial value of the Innas hydraulic transformer. In *The Sixth Scandinavian International Conference on Fluid Power (Tampere, May 26-28 1999, Proceedings)*; University of Tampere: Tampere, Finland, 1999; pp. 873–886.
8. Costa, G.K.; Sepehri, N. Four-Quadrant Analysis and System Design for Single-Rod Hydrostatic Actuators. *J. Dyn. Syst. Meas. Control.* **2018**, *141*, 021011, doi:10.1115/1.4041382.
9. Adams, C. A380: 'More Electric' Aircraft. *Aviation Today*, October 2001.
10. Parker. Compact Electro-Hydraulic Actuator (EHA). 2020. Available online: https://www.parker.com/Literature/Hydraulic%20Pump%20Division/Oildyne%20EHA/Compact-EHA-Catalog-HY22-3101E-7-13.pdf (accessed on 16 November 2020).
11. Actuonix Motion Devices. Miniature Linear Motion Series-L16. 2019. Available online: https://s3.amazonaws.com/actuonix/Actuonix+L16+Datasheet.pdf (accessed on 27 October 2020).
12. Odrive Robotics. Odrive High Performance Motor Control. Available: https://odriverobotics.com/ (accessed on 27 October 2020).
13. Wiens, T.; Deibert, B. A Low-cost Miniature Electrohydrostatic Actuator System. *Actutors* **2020**, *9*, 130; doi:10.3390/act9040130.
14. Bonchis, A.; Corke, P.I.; Rye, D.C. A pressure-based, velocity independent, friction model for asymmetric hydraulic cylinders. In Proceedings of the 1999 IEEE International Conference on Robotics and Automation (Cat. No.99CH36288C), Detroit, Michigan, 10–15 May 1999; doi:10.1109/robot.1999.770361.
15. Caliskan, H.; Balkan, T.; Platin, B.E. A Complete Analysis and a Novel Solution for Instability in Pump Controlled Asymmetric Actuators. *J. Dyn. Syst. Meas. Control.* **2015**, *137*, 091008, doi:10.1115/1.4030544.
16. Wang, L.; Book, W.J.; Huggins, J.D. A Hydraulic Circuit for Single Rod Cylinders. *J. Dyn. Syst. Meas. Control.* **2011**, *134*, 011019, doi:10.1115/1.4004777.
17. Wang, L.; Book, W.J. Using Leakage to Stabilize a Hydraulic Circuit for Pump Controlled Actuators. *J. Dyn. Syst. Meas. Control.* **2013**, *135*, 061007, doi:10.1115/1.4024900.